TROPICAL CYCLONE CHARACTERIZATION VIA NOCTURNAL LOW-LIGHT VISIBLE ILLUMINATION

Jeffrey D. Hawkins, Jeremy E. Solbrig, Steven D. Miller, Melinda Surratt, Thomas F. Lee, Richard L. Bankert, and Kim Richardson

Nighttime visible digital data from the Visible Infrared Imaging Radiometer Suite (VIIRS) have the potential to complement the current infrared imagery standard-bearer in monitoring global tropical cyclone characteristics.

The *Suomi National Polar-Orbiting Partnership* (*SNPP*) satellite was launched on 28 October 2011 and placed into a sun-synchronous afternoon polar orbit (1330 local time ascending node with a corresponding nocturnal 0130 local time descending node). *SNPP* carries a day–night band (DNB) sensor as part of the Visible Infrared Imaging Radiometer Suite (VIIRS). The DNB is a visible (VIS)–near-infrared (IR) passive radiometer, whose special ability to sense extremely low levels of light in the 500–900-nm bandpass provides a unique opportunity to exploit nighttime visible signals for nighttime environmental characterization (Lee et al. 2006; Miller et al. 2013). The improved capabilities hold potentially high relevance to the nocturnal monitoring and characterization of tropical cyclones (TC) within the world's oceanic basins.

Accurately detecting TC structure (rainband organization, eyewall characterization, surface circulation center location, and intensity) in near–real time typically is problematic owing to 1) a scarcity of in situ observations, 2) the spatial and temporal scales involved, and 3) the storm's potential for rapid intensity (RI; >30 kt in 24 h; 1 kt = 0.51 m s^{-1}) changes. These difficulties directly impact the accuracy of TC forecasting on multiple time scales ranging from nowcasts to 7-day forecasts. Improvements to forecasting skill over this wide time frame are critical to a wide range of emergency managers, vulnerable coastal populations, as well as civilian, commercial, and Department of Defense (DoD) interests.

Because of the challenges of monitoring the large data-sparse ocean basins, satellite-based remote

AFFILIATIONS: Hawkins,[a] Surratt, Lee,[a] Bankert, and Richardson—Naval Research Laboratory, Marine Meteorology Division, Monterey, California; Solbrig and Miller—Cooperative Institute for Research of the Atmosphere, Fort Collins, Colorado
[a] Retired
CORRESPONDING AUTHOR: Jeffrey D. Hawkins, jeff.hawkins@sbcglobal.net

The abstract for this article can be found in this issue, following the table of contents.
DOI:10.1175/BAMS-D-16-0281.1

In final form 23 March 2017

sensing, especially geostationary (GEO) infrared, has traditionally provided the backbone of TC observations. GEO satellites provide global coverage and high temporal refresh rates (5–30 min), enabling the creation of such tools as the Dvorak technique (Dvorak 1984), which manually estimates TC intensity via cloud pattern recognition. Objective algorithms such as the advanced Dvorak technique (ADT; Velden et al. 1998; Olander and Velden 2007) followed and have greatly increased the potential temporal sampling since every IR image can now be processed in a few minutes, instead of relying on only manual analyses every 3 or 6 h. However, IR TC views are inherently limited by the inability to see through upper- and midlevel cloud layers. The opacity of most cirrus clouds at IR wavelengths precludes detection of low- and midlevel cloud structure required for storm-center fixes and high-quality intensity estimates. Daytime visible data assist in determining storm structure such as shear (Velden and Sears 2014) when the low-level center is offset from the mid- or upper-level convection and more accurately identify the "scene type" used in the Dvorak method. VIIRS DNB digital data can potentially provide enhanced nighttime data, thus helping to close the gap in accurate intensity estimates.

Microwave sensors (imagers and sounders) in low Earth orbit (LEO) mitigate some of the IR limitations by their ability to view beneath upper-level nonraining clouds and "observe" rain and convection associated with spiral rainbands and inner-core structure that provides critical storm location, intensity, intensity change, and shear data points used both operationally and during field programs and in research studies (Hawkins et al. 2001, 2008; Hawkins and Velden 2011; Turk et al. 2006; Cossuth et al. 2014). Passive microwave (PMW) sensors have been used operationally since 1987's launch of the first Special Sensor Microwave Imager (SSM/I; Hollinger 1989) on the Defense Meteorological Satellite Program (DMSP). These sensors have modest spatial resolution (5–35 km) and swath size (700–1,700 km); thus TC sampling for operational needs has been achieved by utilizing both research and operational sensors over the last two decades to help mitigate the inherent temporal sampling issues associated with any LEO-based sensors. VIIRS DNB products both complement and supplement microwave imager datasets by being able to see through thin cirrus, while at very high spatial resolution.

Denoting the correct surface circulation center is often difficult at night owing to IR imagery issues when dealing with limited thermal contrast between low clouds and ambient sea surface temperatures (SSTs), assuming upper clouds are absent. DNB imagery can often highlight the low-level circulation centers (LLCC) as lunar illumination enables low clouds to be readily identified both qualitatively and quantitatively. These attributes are a major advancement from the heritage nighttime visible sensor on DMSP for the past 40 years, the Operational Linescan System (OLS; Eather 1979), and complement active microwave scatterometer-derived oceanic surface wind vectors that suffer from temporal limitations.

The VIIRS DNB low-light sensor technology provides a new TC observing tool that can mitigate multiple inherent limitations incumbent on GEO/LEO IR instruments (Hawkins et al. 2014). While not available every night owing to the need for sufficient lunar illumination, DNB digital imagery can be frequently incorporated by the TC analyst in determining storm location, intensity, and intensity trends. This paper will outline the unique DNB characteristics that make these observations feasible and compare them with heritage DMSP OLS datasets (Croft 1978) while highlighting the ability to work with uniform quantitative reflectance values instead of wildly varying radiances. The paper will illustrate specific case studies focusing on TC location, structure, and intensity capabilities while also denoting the ability to use night glow (conditions with moon below the horizon) to occasionally capture TC monitoring data. The paper will then highlight some specific near-term future opportunities and then summarize the TC nighttime monitoring skills that the VIIRS DNB can offer the global TC community.

NIGHTTIME VISIBLE SENSING FROM SPACE. While the VIIRS/DNB has garnered considerable attention, the ability to sense low-light visible data has existed for many decades via the DMSP OLS nighttime visible sensor since the late 1960s. The OLS has been used for multiple operational and research missions varying from cloud detection using lunar illumination to population and economic activity surveys via city light emission detection changes (Welch 1980; Elvidge et al. 1997) and lightning studies (Orville 1981; Bankert et al. 2011). The photomultiplier tube used for signal amplification was unique in its coverage of both the visible and near-IR regions of the electromagnetic spectrum (Elvidge et al. 1999). OLS visible data are provided in "smooth mode" during the nighttime, corresponding to a nadir horizontal sampling interval of 2.7 km,

expanding to 5.4 km at the edge of its 3,000-km swath. The OLS has provided researchers and analysts with tantalizing views of cloud layers, tropical cyclones, dust storms, sea ice, snow cover, volcanic plumes, and other phenomena. However, fundamental limitations of the OLS instrument including a lack of onboard calibration, only 6-bit digitization (64 observable radiance ranges), and issues with stray light entering the sensor limit analyses to subjective human interpretation.

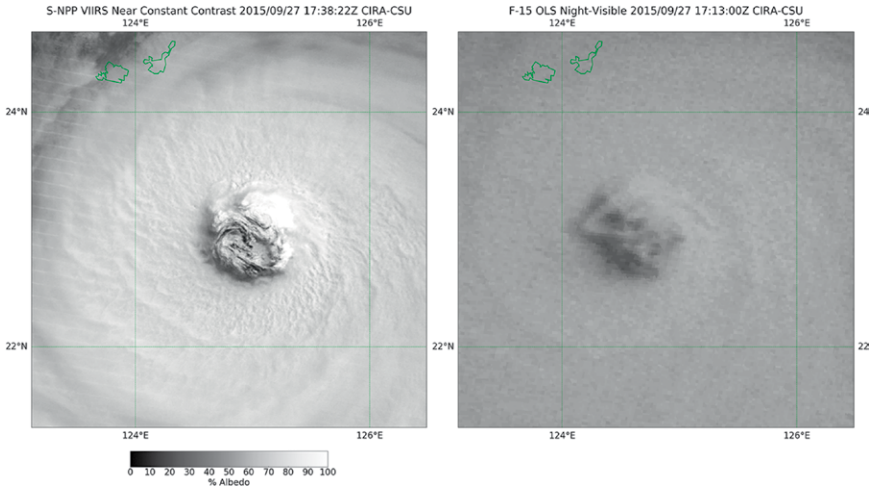

Fig. 1. TC eye and eyewall structure as viewed by a (left) VIIRS DNB near-constant-contrast (NCC) product (1738 UTC) and (right) DMSP OLS nighttime visible radiance image (1713 UTC) for western Pacific Typhoon Dujuan (21W) on 17 Sep 2015. Note the ability in the DNB product to discern mesovortices inside the eye, while analysts would be hard-pressed to extract the relevant details in the coincident OLS imagery.

Through its innovation to the heritage OLS design, the VIIRS DNB provides a wealth of advantages (Lee et al. 2006; Hillger et al. 2015). These advantages include 1) on-orbit calibration versus no active calibration for OLS (Mills et al. 2010), 2) 13–14-bit (~8,000–16,000 levels) versus 6-bit (64 levels) digitization (Liang et al. 2014), 3) improved handling of dynamic radiance changes across the terminator via a third gain stage, and 4) enhanced spatial resolution of 0.742 km across the 3,000-km swath (Schueler et al. 2013). When considering the horizontal spatial resolution of OLS is ~5 km (but sampled horizontally to report 2.7-km "pixels"), the DNB pixels are roughly 45 times smaller than OLS at nadir and 90 times smaller at edge of scan (Miller et al. 2013). These attributes enable the user to both qualitatively and quantitatively use DNB data in a manner not feasible with OLS data for all the applications noted in the prior publications. This paper focuses on the specific TC monitoring advances enabled by this new technology.

Figure 1 highlights these key fundamental advantages of VIIRS DNB versus OLS, where the right panel displays a grainy OLS view of Typhoon Dujuan at 1713 UTC 27 September 2015 under very good lunar illumination. On the left, the nearly coincident VIIRS DNB image at 1738 UTC enables the user to leverage the sensor's superior capabilities: 1) better resolution and digitization resolves features that are fuzzy in the OLS data such as eye mesovortices (Kossin et al. 2002), 2) dramatically improved digitization and reduced noise permits feature extraction within upper-level cirrus, and 3) enhancements in both spatial and radiometric resolution permit mapping of the number and location of overshooting tops that may be tied to storm intensity.

Figure 1 shows a scene with nearly a full moon and thus optimal conditions for nighttime visible imagery. Miller et al. (2012a) calculate the lunar availability for several polar orbits, noting that while roughly 40%–50% of all nighttime observations (annual average) in the tropics will provide some level of moonlight to work with, only about 20% of all night observations will provide the moonlight levels seen in Fig. 1. As noted in Lee et al. (2006), the moon's lunar illumination varies by a nonlinear function of 9 times from full moon to first- or third-quarter moon. This extreme range causes difficulty when attempting to use OLS nighttime visible data since there is no viable method to "correct" the observed radiances into top-of-the-atmosphere (TOA) reflectances and thus provide consistent lunar information from image to image, or from night to night. Therefore, OLS analysts hoping to gain meteorological insight could only use a very small time window (4–5 days) within the lunar cycle straddling the full moon, when lunar moonlight was strong enough to discern clouds from the land/ocean background, further limiting TC monitoring utility.

CONVERTING RADIANCE TO REFLECTANCE. DMSP OLS nighttime visible imagery is often difficult to interpret owing to the ever-changing lunar conditions and the inability

to work quantitatively with the data. Thus, qualitative analyses are the norm, and even they are problematic since expert analysts are needed to extract meaningful information. Miller and Turner (2009) outline how VIIRS DNB radiances can be accurately converted to TOA reflectances via use of a "lunar model" and the DNB spectral response function. Computing reflectance involves normalizing the highly variable radiance by the amount of incoming moonlight (from the model), thus creating a standard parameter whose attributes benefit both subjective and objective analyses. Using state-of-the-art solar source observations and lunar spectral albedo data and accounting for the time-varying sun, Earth, and moon geometry and lunar phase, the model produces downwelling TOA lunar irradiance spectra over the interval [0.3, 1.2] μm for a given date and time. These spectra are convolved with the DNB sensor response function, permitting the conversion from upwelling radiance to equivalent lunar reflectance (i.e., 0%–100%).

Miller et al. (2013) illustrate application of the lunar model to a TC example (Typhoon Jelawat) that is reproduced here in Fig. 2. For this case, which occurred across the "lunar terminator," the lunar reflectance conversion enhances the faint and spatially varying nighttime visible signals to reveal detailed TC structure. The reflectance imagery highlights Jelawat's cyclonic spiral rainbands, overshooting convective cloud tops embedded within the rainbands, the inner core, or eyewall structure surrounding the clear eye and, in general, structural details that one normally attributes to daytime visible imagery. The moon is setting to the west and nighttime city lights can be seen on Taiwan to the northwest and lightning over the Philippines and northeast of the eyewall (Fig. 2a). Creating the reflectance product is automated using lookup tables and takes less than a minute on modern workstations.

DMSP OLS nighttime visible imagery can only be used under optimum lunar conditions, typically lasting only 4–5 days. Because of its significantly higher dynamic range, radiometric resolution, and ability to be converted to reflectance due to onboard calibration, VIIRS DNB data can increase this usable moonlight period by a factor of 2–3, to 12–14 days. Given the sensitivity of the DNB, moonlight imagery can be rendered for any nighttime pass when the moon is above the horizon and is at crescent phase or higher. Since *SNPP* is in a sun-synchronous orbit, but the lunar cycle spans ~29.5 days, the DNB provides an asynchronous sampling of the lunar cycle. For the specific geometry of the 0130 *SNPP* orbit, the moon is above the horizon from roughly two nights after first quarter until two nights after last quarter phase (Miller et al. 2012a, 2013). The peak lunar irradiance thus occurs on the two nights immediately following the full moon, during the waning gibbous phase. Although the lunar disk is not as fully illuminated, the amount of moonlight is higher because the moon is higher in the sky at 0130 local time on these nights.

The improved span of lunar imagery availability for the DNB is captured in Fig. 3 for Hurricane Julio from 7 to 15 August 2014. DNB reflectance imagery for nine consecutive nights (left portion of each panel) clearly reveals the slow increase in lunar illumination the DNB can sense and begin to depict TC cloud features. Meanwhile, nearly coincident DMSP OLS nighttime visible radiance imagery (right portion of each panel) is simply unable to depict any cloud structure early on under very-low-light conditions at the start and end of this sequence. In the top-middle panel of Fig. 3, the lunar source function provides sufficient lighting for the OLS sensor to highlight

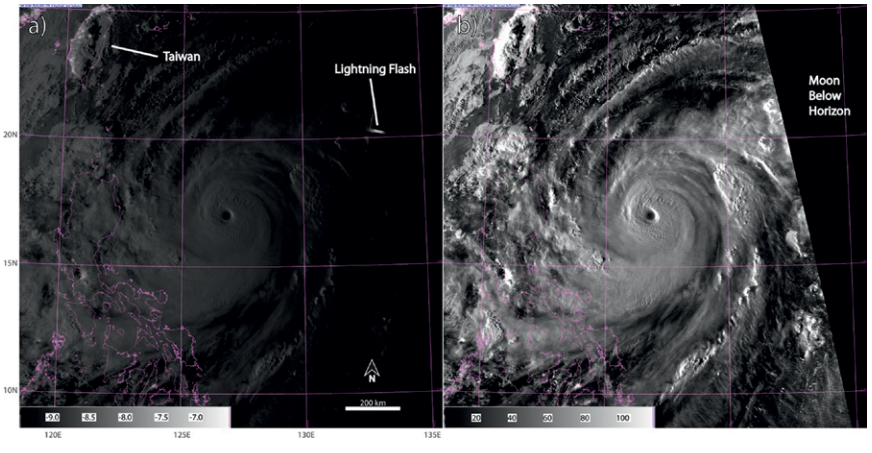

Fig. 2. Western Pacific Typhoon Jelawat (18W) at 1702 UTC 25 Sep 2012 (140-kt intensity) as viewed by (a) VIIRS DNP radiances and (b) lunar-model-corrected reflectances. The moon is setting to the west in (a), and low illumination values across the eastern half of the storm can be accurately adjusted to full-moon conditions, thus greatly enhancing the TC structures (cf. Fig. 3 from Miller et al. 2013).

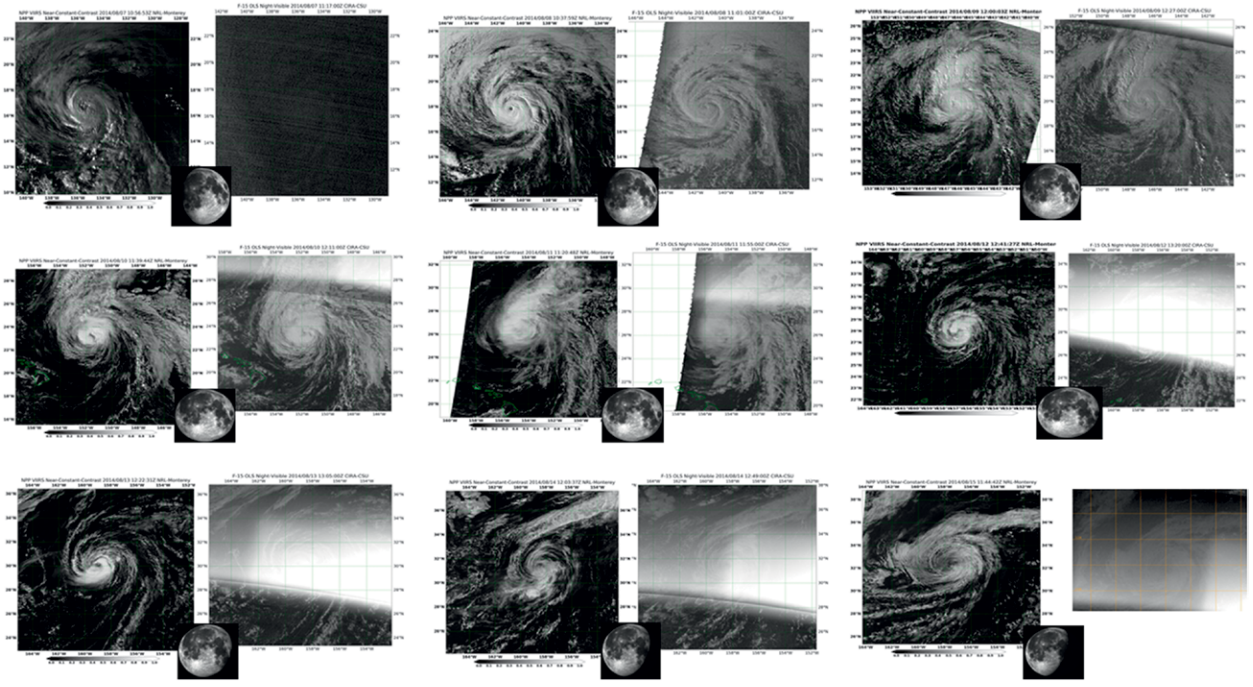

Fig. 3. A sequence of VIIRS DNB imagery on nine consecutive nights (7–15 Aug 2014) for Hurricane Julio (10E) comparing DNB NCC imagery (left portion of each panel) to coincident OLS nighttime visible radiances (right portion of each panel). Note the inability of the OLS to observe any TC cloud features early on owing to insufficient lunar lighting while DNB captures relevant storm structure. In addition, persistent issues with solar glare in OLS products can frequently degrade the ability to view TC features. A lunar-phase graphic is included in the bottom center of each example.

clouds, but the degree of clarity that could be utilized for either qualitative or quantitative applications is orders of magnitude poorer than the DNB digital dataset. Additionally, starting on 10 August (Fig. 3, left-middle panel), contamination from stray light entering the OLS sensor from the sun begins to encroach on the image domain, heavily obscures the storm center by 12 August (Fig. 3, right-middle panel), and remains a problem through 15 August. Thus, the combined capability of DNB to physically sense TC clouds over a longer time frame during the lunar cycle, and its inherently enhanced ability for depicting cloud structure is a boon for nighttime TC structure analyses. These analyses can be focused on finding surface circulation centers, highlighting convective organization and intensity changes. Techniques such as the ADT and the automated rotational center hurricane eye retrieval (ARCHER; Wimmers and Velden 2010, 2016) utilize IR imagery to extract key storm features, providing critical guidance to TC warning agencies about changing storm structure. The reflectance information can also be combined with coincident IR data for multisensor TC intensity estimates. Thus, nighttime visible data have the potential to assist Dvorak-type intensity analyses as done during solar illumination. At full resolution, the reflectance imagery is an excellent tool for mapping overshooting tops, which have been noted to be associated with rapid intensity changes when near the inner core by multiple authors, including Simpson et al. (1998).

SNPP VIIRS DNB TC EXAMPLES. *Peering through cirrus.* TCs are frequently associated with intense convection, which creates an upper-level "central dense overcast" (CDO) condition that shields VIS–IR sensors from viewing mid- or low-level cloud structure. Our inability to "see through" upper-level clouds and map storm structure is a key GEO dataset limitation and a fundamental reason why passive microwave imagery is used in TC monitoring efforts globally (Hawkins et al. 2001; Lee et al. 2002). CDOs often have thick opaque cirrus canopies, but a subset of cases has thin cirrus, which DNB data can see through to the underlying clouds, owing to the highly scattering nature of visible light. Lunar illumination thus permits us to see through the thin cirrus to the low-level clouds spiraling cyclonically into the storm center that may not be aligned with the mid- to upper-level IR center.

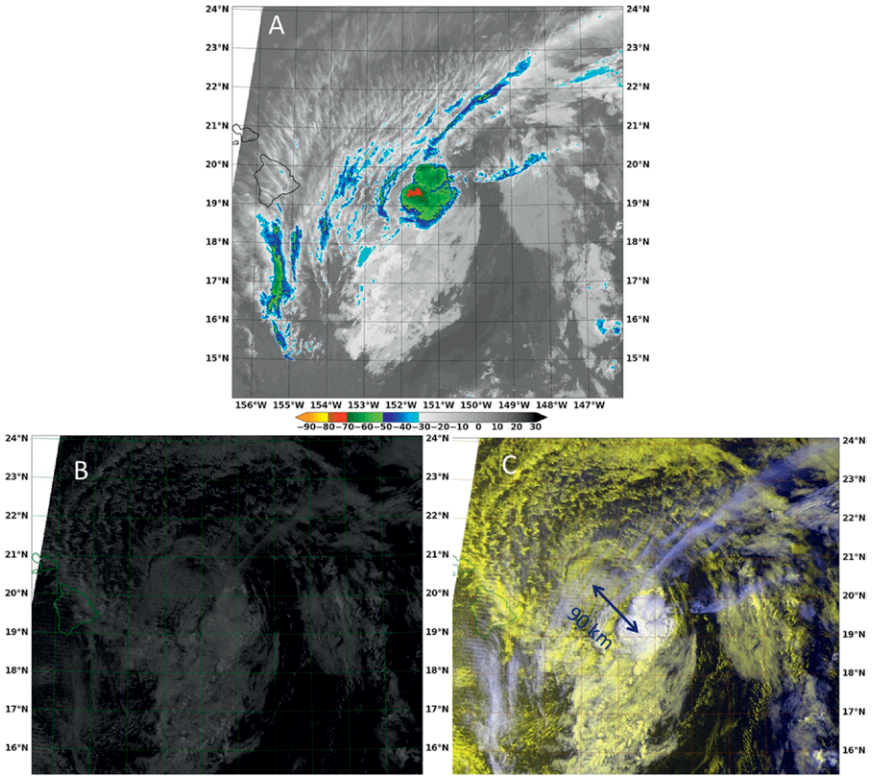

Fig. 4. Eastern Pacific Tropical Storm Flossie at 1102 UTC 29 Jul 2013 as viewed by (a) VIIRS longwave IR (colder, higher clouds are colored according to the scale), (b) DNB nighttime visible radiances, and (c) DNB RGB product using reflectances and IR digital data. Note the benefits of combining the corrected reflectances and longwave IR in an RGB product that enhances the ability to comprehend the 3D structure. The low-level center in (c) is at the northwest end of the two-pronged arrow, while the midlevel center is at the southeast end. The prominent cirrus outflow in the IR image precludes the ability to view the LLCC below as evident in the coincident DNB data.

Figure 4 highlights a case where monitoring only the nighttime IR "circulation center" can lead to an inaccurate center fix and intensity errors. Figure 4 shows the VIIRS 11-μm longwave-IR image (Fig. 4a) of Tropical Storm Flossie at 1102 UTC 29 July 2013. The color table for the cloud-top temperatures maps cold (high) values as red and green and warm (lower) clouds as light white and/or gray. At the *SNPP* overpass time, Flossie was composed mostly of low-level clouds to the south and east of the apparent "green–red" center of mass and dominated by cirrus clouds in the northern semicircle radiating outward, driven by the anticyclone aloft. Animating coincident Geostationary Operational Environmental Satellite (GOES)-West IR data (not shown) provided analysts at the Central Pacific Hurricane Center (CPHC; Honolulu, Hawaii) with a consistent westward-moving time series. Forecasters used the GEO IR imagery and models to forecast landfall on the Big Island of Hawaii, and the multiday track carried Flossie south of the islands (Maui and Oahu), exposing them to the stronger winds in the northern semicircle. However, DNB imagery (Figs. 4b,c) revealed that the CPHC best track center was displaced from the true LLCC, farther northwest.

Multispectral DNB-enhanced imagery. Exposed LLCCs (without overriding cirrus) are often difficult to observe with IR imagery alone, owing to the poor temperature contrast between the warm cloud-top values and the underlying SSTs (Lee 2000). Figure 4 further simplifies the analyst's ability to interpret TC structure by combining DNB reflectances with coincident longwave IR to create a red–green–blue (RGB) color composite. The red and green color guns use the DNB reflectance product, while the blue gun holds the IR imagery (inverted, so that cold pixels have strongest blue saturation). This combination depicts low-level clouds in yellow and upper-level clouds in white (thick) or blue (thin). As shown in previous examples, the conversion from DNB radiances to reflectances helps to enhance the low-level cloud field. By leveraging the IR dataset, the optically thin nature of the cirrus shield is revealed—information that is lost to the IR (Fig. 4a) where these same clouds are opaque. Most importantly, Fig. 4c clearly reveals a ~90-km displacement between the surface (DNB detected) and upper-level (IR detected) circulation centers caused by shear. Inadequate knowledge of the shear when using IR-only imagery leads not only to poor track forecasts but also to intensity estimate errors since knowledge of shear is a critical aspect in Dvorak intensity analyses. Thus, analysts placed Flossie too far south and with an intensity that is too strong when using the incorrect IR-based center position. CPHC forecasters then leveraged the DNB data to issue a special advisory with significant track and intensity changes:

The center of Flossie was hidden by high clouds most of the night before VIIRS nighttime visual satellite imagery revealed an exposed low level circulation center farther north than expected. We re-bested the 0600 UTC position based on the visible data. —National Weather Service Central Pacific Hurricane Center, Honolulu, Hawaii, Monday, 0500 Hawaii Standard Time (HST) 29 July 2013

DNB data also aid analysts in defining the low-level wind field, especially when used in concert with ocean surface wind vectors from microwave scatterometers [Advanced Scatterometer (ASCAT; Figa-Saldana et al. 2002), Oceansat Scatterometer (OSCAT) onboard *OceanSat-2* and Rapid Scatterometer (RapidSCAT)] and the WindSat polarimetric radiometer (Gaiser et al. 2004). Figure 5 shows scatterometer data for Flossie overlain on a *GOES-15* IR image. A closed circulation in the surface winds agrees with the DNB and positions the center northwest of the IR convective cloud tops. Winds are weak, but winds of 40+ kt are northeast of center, typically the strongest for TCs moving to the west-northwest. These surface winds are also validated in ASCAT wind vectors (not shown). However, owing to the limited swath and scatterometer LEO orbit, this valuable dataset is only infrequently available; thus DNB is highly complementary. This offset between the LLCC and the mid- to upper-level clouds and rain center are also verified in coincident passive microwave imager digital data. An F-18 Special Sensor Microwave Imager/Sounder (SSMIS) overpass at 0617 UTC (~3 h before *Oceansat-2*) clearly depicts a similar configuration when viewing the 91-GHz "color composite" product. Heavy cloud liquid water (light blue–white color) is denoted in the red circle encompassing the storm center, while red colors are associated with rain and frozen hydrometeors, which heavily scattered the signal, depressing brightness temperatures T_B. Passive microwave data are temporally limited owing to their LEO hosts (twice-per-day potential views), thus complementing scatterometer data in defining accurate LLCC positions. Thus, DNB and microwave scatterometer and imager data can assist VIS–IR in fixing storm centers and create higher-fidelity storm warnings.

Figure 6 illustrates this center vertical alignment problem with Tropical Depression 30W after it crossed from the western Pacific into the Indian Ocean (IO) between Sri Lanka and India on 15 November 2013. The VIIRS IR product denotes strong convection near the coast (red–green high cloud tops; left panel), while the DNB + IR RGB imagery (right panel) reveals an exposed LLCC that is elongated northwest–southeast with convection near the northwest edge. Knowledge of the LLCC position, size, orientation, and position relative to the main convection and changes in that relative positioning from the previous evening are critical to creating accurate warning messages. As noted by Hillger et al. (2015), the Joint Typhoon Warning Center has used the low-level flow pattern via animations to estimate the locations of LLCCs more accurately than when using IR imagery alone, even when the LLCC itself is obscured. Poor center positions and intensity estimates (Dvorak keys on shear scenes differently than nonshear) would negatively impact bogus vortex details provided to both regional and global NWP models (Kurihara et al. 1993; Leslie and Holland 1995). These intensity errors would likely vary from 10 to 25 kt, maybe more in extreme cases, and would directly change watches and warnings that impact the extensive TC warning recipients.

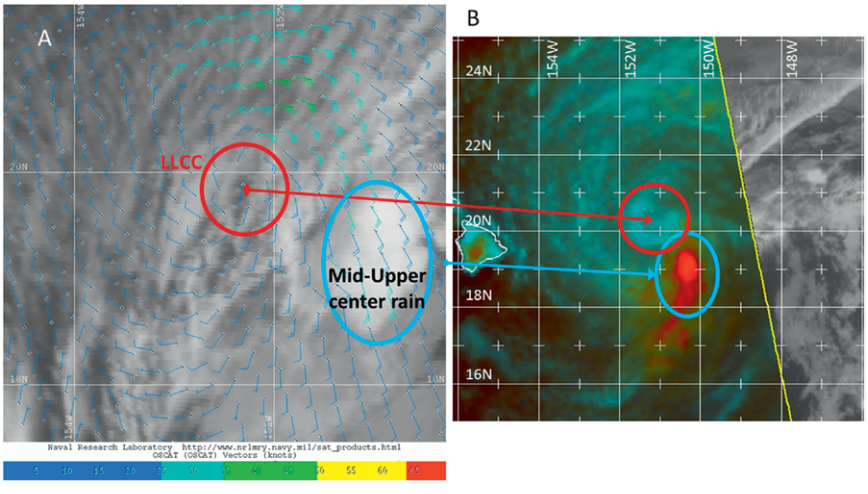

Fig. 5. (a) Eastern Pacific Hurricane Flossie ocean surface vector winds as determined by India's *Oceansat-2* scatterometer at 0956 UTC 29 Jul 2013, overlain on a *GOES-15* (GOES-West) IR image (0930 UTC) as the storm is approaching the Hawaiian Islands. (b) Passive microwave imager (F-18 SSMIS) 91-GHz "color composite" product at 0617 UTC, 3 h earlier, highlighting the separation of the LLCC and mid- to upper-level rain center.

Figure 7 illustrates the commonly occurring case when the upper- and midlevel clouds are sheared away completely, revealing a well-defined exposed LLCC as noted in an OLS nighttime visible (left panel; 0556 UTC) and VIIRS DNB reflectance imagery (right panel; 0517 UTC) for Tropical Storm Humberto on 17 September 2013. Neither image product has been enhanced in any specific way, readily showcasing the reflectance image capability to mitigate the low-light levels in the OLS dataset and capture storm cloud structure throughout the scene, not just the LLCC clearly seen in both datasets. The OLS image captures multiple lightning pulses while VIIRS enables the user to see cloud details at all levels, not just low-level circulation features.

Convective bursts, overshooting tops. The number of convective bursts and their location relative to the LLCC is important in determining current and near-term storm intensity. Multiple studies have examined these "convective hot towers" in TCs and generally conclude that they play an important role in the dynamics of short-term intensity trends and thus need to be monitored to improve our understanding and ability to predict storm evolution (Malkus 1959; Simpson et al. 1998; Zipser 2003; Hendricks et al. 2004). Observing hot towers via satellite remote sensing is problematic since GEO sensors are limited to VIS–IR channels, and upper-level clouds often mask underlying convective cells that have yet to overshoot the CDO. In addition, generally coarse GEO IR spatial resolutions (~4 km at nadir until Himawari-8 and GOES-R, then 2 km) limit our ability to pinpoint these initial bursts. Microwave imagers, especially those with higher spatial resolution [Advanced Microwave Scanning Radiometer 2 (AMSR2), Global Precipitation Measurement (GPM) Microwave Imager (GMI), and WindSat] can assist with this problem, but their temporal sampling is inadequate. The VIIRS DNB/IR false-color-imagery product described previously can aid this effort, albeit with the same sampling limitations as the microwave imagers given SNPP's LEO.

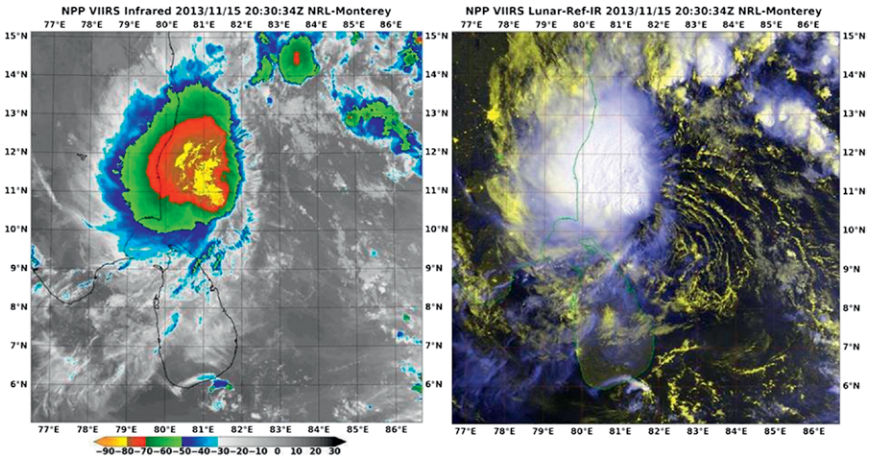

Fig. 6. Bay of Bengal Tropical Depression 30W on 15 Nov 2013: (left) VIIRS longwave-IR and (right) DNB + IR RGB images. Note the definition of the elongated (northwest–southeast) low-level circulation center, the position of the deep convection near the northwest edge of the LLCC, and the inability to view similar features in the IR data.

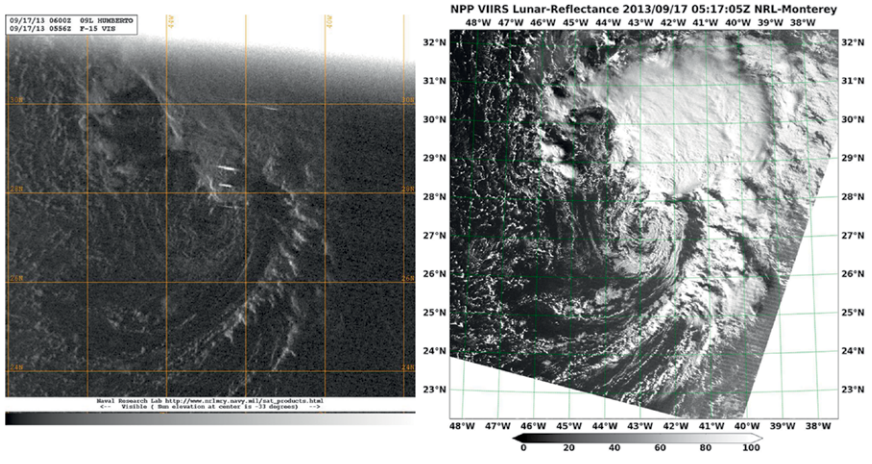

Fig. 7. (left) OLS nighttime visible imagery (0556 UTC) and (right) VIIRS DNB reflectance imagery (0517 UTC) for Atlantic Tropical Storm Humberto on 17 Sep 2013. These products showcase the reflectance image capability to mitigate the OLS low-light levels and capture storm cloud structure including both the exposed LLCC and highly asymmetric upper-cloud organization.

Figure 8 depicts how the enhanced DNB + IR false-color imagery can help isolate overshooting tops, both in the inner core and rainbands. While the DNB + IR false-color technique is typically used

to view through thin cirrus clouds aloft and capture convective cells below, it can also be modified to enhance overshooting tops with cold cloud tops. In these images, the thresholds used for the inverted IR in the blue channel are modified to only encompass very cold cloud tops (180–230 K rather than 200–300 K), making use of the IR channel's high radiometric resolution. This provides contrast between cold and very cold cloud tops at the expense of the warm clouds. Additionally, when the lunar geometry provides strong side illumination of overshooting tops, important structural details can be observed owing to high contrast between bright, illuminated overshooting tops and the shadows they cast on neighboring clouds. It should be noted that both OLS and VIIRS can do an admirable job viewing overshooting tops for "first light" or "last light" scenes if both were in the DMSP terminator orbital plane.

Tracking the life cycle of TCs. TC eye genesis and structural changes are fundamental features every warning center monitors, but clouds and poor thermal contrast can preclude IR views. Here, the DNB can assist in all phases of the TC life cycle. Figure 9 highlights a suite of nightly images using the standard DNB + IR enhancement for Hurricane Andres as we map eyewall formation and subsequent decay over 5 nights. The second image has a cloud-free eye, followed by shearing between the low and upper levels and then emergence of the LLCC as identified by the yellow low-level cloud field as convection dissipates and the storm circulation spins down.

Improved wide-swath coverage. The 3,000-km DNB swath exceeds the minimum coverage needed to ensure overlap between successive orbits, even at the equator (~2,800 km). This factoid is typically not valued or fully understood since most VIS/IR sensors are cross-track scanners whose field of view grows significantly from nadir to the scan edge. VIIRS mitigates this issue through a novel detector

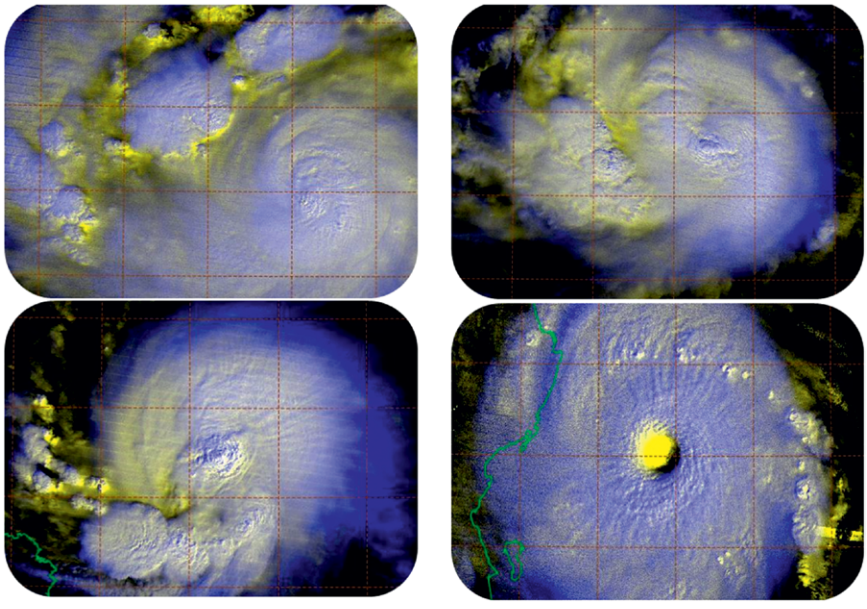

Fig. 8. Sequence of four DNB + IR RGB composites (once per night) as western Pacific Typhoon Noul intensifies (80–130 kt) from 6 to 9 May 2015 as it approached the Philippine Islands, highlighting overshooting tops associated with spiraling rainbands and organized convective activity penetrating the upper-level cirrus canopy.

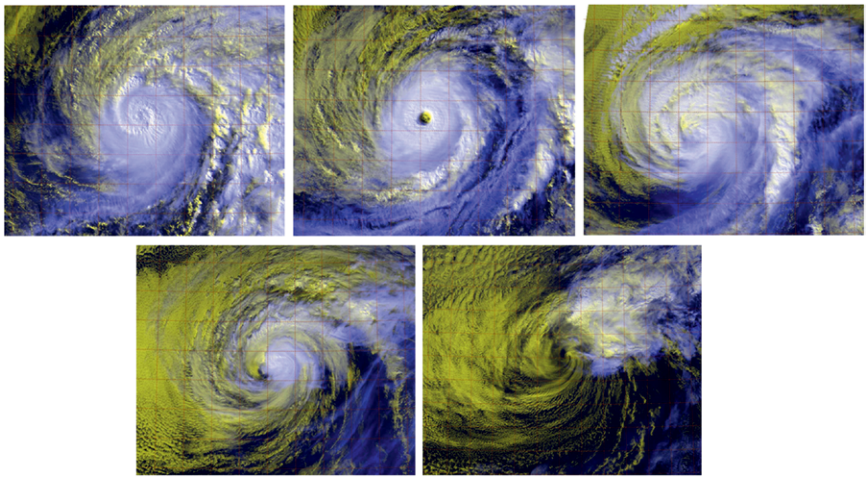

Fig. 9. Once a night view of eastern Pacific Hurricane Andres during 31 May–4 Jun 2015 using DNB + IR RGB composites (white-cyan indicates mid- to upper-level convective clouds and yellow indicates lower-level stratus). Low-level stratus dominates the scene once the convection wanes and is sheared to the northeast. Images contain 1° × 1° latitude–longitude squares.

aggregation technique (Schueler et al. 2013), thus permitting imagery at the swath edge with excellent spatial details, and for successive passes, to be leveraged in examining temporal changes.

Figure 10 includes consecutive orbital imagery, enabled by the overlap of successive orbits, for western Pacific Typhoon Linfa (10W) on 6 July 2015. These occurrences of overlapping day and nighttime passes uniquely highlight TC environment fluctuations over the ~100-min duration between adjacent orbits. The daytime visible imagery (top panel) outlines significant redevelopment of convection near the exposed LLCC. The shear was relaxing and the deep convection was redeveloping near the center. The nighttime images (bottom panel) capture evolution of the low-level cloud field north and northeast of the TC center in addition to changes in overshooting tops located mainly south of the surface center. Isolated along-scan bright segments correspond to lightning activity occurring at the instant of *SNPP* (Bankert et al. 2011), centered on the robust mesoscale convective complex near the storm's mid- to upper-level center. In general, positive detection of lightning activity by the DNB (which is a nonstaring, whisk-broom sensor) is an indication of considerable storm electrification.

Nightglow sensing. Up to this point, our discussion has concentrated on the use of DNB lunar reflectance to highlight TC features. However, the DNB also holds a limited ability to detect optically thick cloud on nights *without* moonlight—providing a means to monitor some of these same aspects of TC structure any night. Miller et al. (2012b) describe the unexpected capability of the DNB to sense the faint atmospheric chemiluminescent emissions known as airglow. The main sources of nightglow (encompassing the subset of airglow production mechanisms occurring at night) within the DNB bandpass originate from excited-state hydroxyl (OH*), which include emission lines growing in intensity toward the near-IR. These nightglow emissions occur from the upper mesosphere to the middle thermosphere and originate principally from a ~10-km-thick region near the mesopause (~90 km above mean sea level). Nightglow acts effectively as a "pan-horizon" source of nondirectional downward illumination to the lower atmosphere. The intensity of these emissions is 100–1,000 times weaker than lunar illumination, but the DNB's sensitivity detects these signals at or just above the observation noise floor (around 3×10^{-7} W m^{-2} sr^{-1}). On nights with moonlight, nightglow plays a negligible role in the scene radiance.

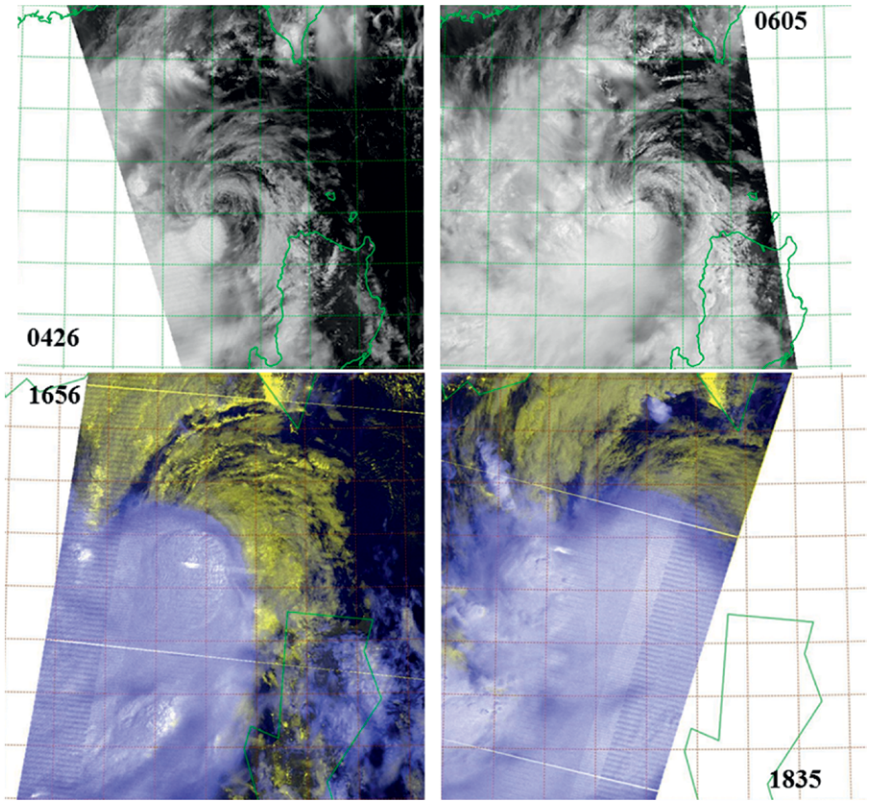

Fig. 10. VIIRS DNB imagery of western Pacific Typhoon Linfa (10W) on 6 Jul (top) daytime passes (0426 and 0605 UTC) and (bottom) nighttime passes (1656 and 1835 UTC) depicting the overlap between successive passes due to the 3,000-km swath width.

Figure 11 shows an example of IR and DNB + IR composite imagery of Supertyphoon Sanba at ~1650 UTC 15 September 2012 as the storm nears Okinawa. This pass occurred one night after the new moon, when the moon was well below the horizon. Despite the total lack of moonlight, the extensive cloud field associated with Sanba is well depicted owing to nightglow reflection. The bright city lights of China, Taiwan, South Korea, and Japan are far removed and below the horizon with respect to most of this system, and

there are no discernible indications of surface-based illumination (e.g., strong side illumination, 3D effects, and gradients of decreased brightness away from cities). In contrast to lunar or solar reflectance, the nightglow imagery takes on an appearance reminiscent of IR imagery since the light source is pan-directional (eliminating shadows). This characteristic of nightglow illumination renders it perhaps less useful for analyzing storm-top structure, such as overshooting tops, since the relief effects due to shadowing are minimal.

While the ability to sense cloud-top structure may be compromised, nightglow DNB imagery retains a unique ability to peer through optically thin cirrus to reveal the LLCC of strongly sheared TC systems with overriding cirrus. It can, in fact, be applied to the same IR multispectral technique demonstrated in previous examples. Figure 12 demonstrates the DNB + IR RGB imagery for TC Dolores on a new moon night. The appearance of the imagery is reminiscent of the lunar illumination examples, although some textural details of the low cloud field (yellow) are lost owing to the inherently noisy nature of the nightglow measurements, which reside near the noise floor of the DNB. Nonetheless, useful information content is present. Dolores is in a weakening stage with evidence of strong shear that is decoupling the lower and upper circulation. The nightglow reflectance off low liquid-phase clouds is feasible since cirrus clouds are highly forward scattering at the wavelengths comprising the DNB bandpass.

The nightglow emissions, being isotropic, also emit upward into space, and in some instances these direct emissions can be detected in DNB imagery. The spatially homogeneous nature of most nightglow (brightness features varying over scales of thousands of kilometers) results in a general "milky" appearance, with slight enhancement toward the edges of scan due to longer optical paths through the nightglow layer. However, finescale (on the order of tens of kilometers) modulations to the nightglow layer properties by the passage of atmospheric gravity waves are also present and readily apparent. Yue et al. (2014) and Miller et al. (2015) demonstrate how gravity waves launched by vigorous TC convection produce complex patterns in the direct upwelling emissions sensed by the DNB. An example of this phenomenon is shown in Fig. 13 for Typhoon Koppu at ~1700 UTC 15 October 2015. Koppu's deep, intense convection launched a train of gravity waves into the upper atmosphere, and the concentric ring pattern captures their passage through the nightglow layer. These waves take over an hour to reach the mesopause emission level and

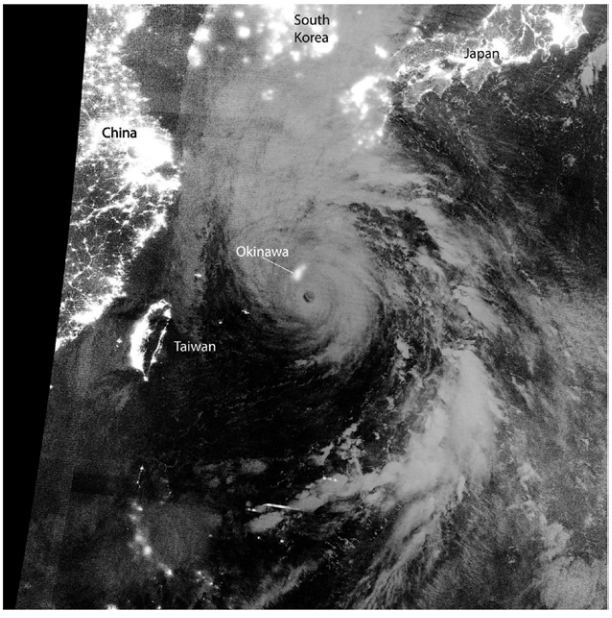

Fig. 11. VIIRS DNB imagery of western Pacific Typhoon Sanba collected at 1650 UTC 15 Sep 2012. On this night, close to the new moon, there is no moonlight illuminating the scene—clouds are detectable via reflection of downwelling hydroxyl nightglow emitting principally from a region near the mesopause.

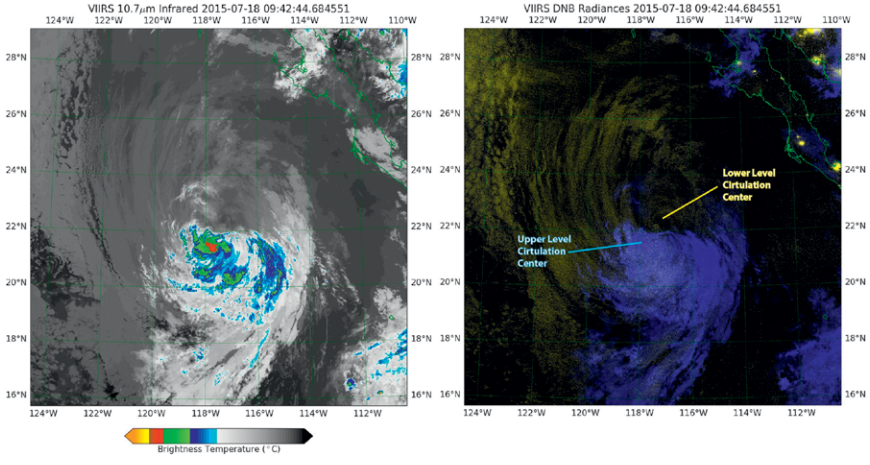

Fig. 12. (left) VIIRS IR and (right) DNB+IR RGB composite imagery of eastern Pacific TC Dolores, collected at 0942 UTC 18 Jul 2015. Details of the LLCC are inferred from the yellow-enhanced clouds, illuminated in this case by atmospheric nightglow as in Fig. 11.

must traverse the stratosphere and mesosphere, which process the wave energy (absorption, breaking, and other effects) via wind shear and critical layers (e.g., Alexander et al. 2010). The relationship between observed waves, their spatial extent and structure, and TC activity/evolution are poorly understood and of potential interest for future investigation.

Emergent DNB TC analysis tools. DMSP OLS nighttime visible imagery was infrequently used qualitatively due to inherent limitations. VIIRS DNB digital data remove these shackles and greatly expand the potential of mitigating nighttime IR TC monitoring via lunar illumination, both qualitatively and quantitatively. The options available after successfully creating accurate reflectances versus widely varying radiances benefit the satellite analyst and enable objective techniques that can directly aid existing methods such as the center fixes. Center fixes are a key first step on any TC satellite analysis since the Dvorak method relies heavily on knowing if shear is occurring, and if so, different logic is followed on categorizing cloud organization. DNB's ability to detect LLCC during shear could be routinely used in a modified version of the Cooperative Institute for Meteorological Satellite Studies (CIMSS)-developed ARCHER technique. The creation of spiral and ring scores created from DNB reflectance digital imagery could prove advantageous when done in conjunction with coincident IR datasets. ARCHER could utilize the DNB reflectances to capture the surface circulation when coincident IR is problematic. This leveraging of DNB surface fixes could then aid ADT values by accurately adding this shear information to the current storm attributes.

Multiple methods exist to exploit IR imagery to identify and monitor the location relative to the center and organization of overshooting tops via IR datasets. DNB datasets can complement this effort by using reflectance imagery to help accurately isolate these vigorous convective elements that may be related to short- and long-term intensity variations. Automated programs can be applied that would intercompare both IR and DNB values and leverage their capabilities to produce a higher-quality product. This would obviously take on added promise if the DNB sensor were on additional LEO platforms such as the European Organisation for the Exploitation of Meteorological Satellites's (EUMETSAT) 0930 LTAN midmorning orbit, or more importantly, when adapted to a GEO reference point.

SUMMARY AND CONCLUSIONS. The VIIRS DNB sensor has made good on promises to radically improve the monitoring of tropical cyclones beyond the capabilities of the DMSP OLS nighttime visible sensor as a result of significant advances associated with sensor calibration, radiometric digitization, low signal-to-noise ratio, and higher spatial resolution. The combination of onboard calibration, 13–14-bit digitization, and 0.742-km spatial resolution across the entire 3,000-km swath enables the TC community to more fully exploit nighttime visible data. Using lunar reflectance off the tops of clouds at multiple levels, DNB imagery can be combined with IR imagery to effectively highlight TC vertical structural details that are otherwise difficult or impossible to observe using coincident IR datasets alone, whether from GEO or LEO platforms.

As shown in this paper, the DNB can readily probe through thin upper-level cirrus to observe critical LLCC features below, which is not feasible in coincident IR, routinely capture storm shear evolution as the LLCC separates from the convection at mid- to upper levels, and assist in isolating overshooting cloud tops important for monitoring TC eye formation and predicting short-term intensity changes, eyewall genesis, and structure changes. The ability to easily visualize shear via blended DNB/IR enhancements is especially important since the majority of TCs experience shear during their lifespan. The unique capabilities

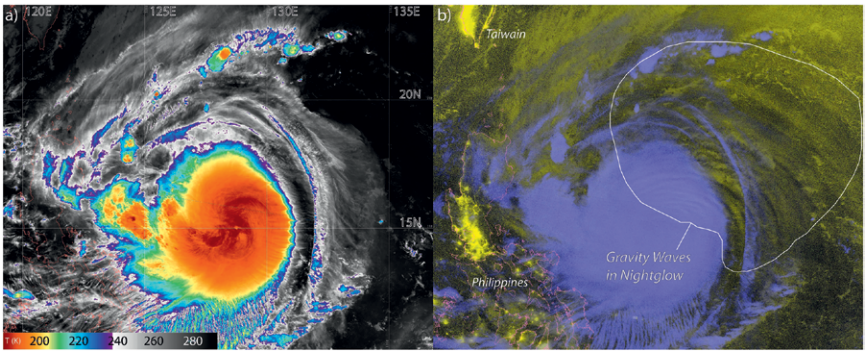

Fig. 13. (left) VIIRS IR and (right) DNB + IR RGB composite imagery of western Pacific TC Koppu collected at 1700 UTC 15 Oct 2015. Within the white-outlined region are DNB-detected mesospheric nightglow emissions showing a train of concentric gravity waves (yellow banded structures) radiating from above the TC and propagating to the northeast.

mitigate multiple inherent limitations associated with nighttime IR data such as the low thermal contrast and modest spatial resolutions, especially with GEO sensors. IR shear capabilities are at the heart of fundamental issues with the Dvorak methodology (Velden et al. 2006). Here, DNB data can help fill in the gaps and work in a multispectral data fusion manner. The DNB/IR imagery products also provide a powerful tool to both subjective human analysts and the rapidly growing list of automated quantitative guidance tools.

By leveraging a lunar irradiance model for conversion to reflectances and taking advantage of the DNB's calibrated data, TC monitoring via moonlight is now possible for 14–15 days per lunar cycle, instead of ~4–5 days using older-technology DMSP OLS imagery. This threefold extension of temporal sampling can then be combined with the consistent top-of-the-atmosphere reflectance products to provide the stable digital datasets required for objective algorithms to extract TC storm features, whether used by themselves or in multichannel or multisensor combinations. These attributes are an essential building block to creating a viable tool for global TC monitoring and hold promise for future LEO and/or GEO nighttime visible sensors that would enhance the temporal sampling.

During the lunar cycle period when moonlight is not available, the DNB continues to provide a form of visible light imaging via nightglow illumination, enabling similar capabilities to locate the LLCC via low cloud spirals residing beneath overriding thin cirrus, while also revealing upper-atmospheric wave structures that are tied to TC convection and contain information content on the above-storm environment that may bear relevance to TC evolution. Overall, the DNB brings to the TC forecasting community a unique and powerful new tool for tracking and warning the public on nature's most powerful storms. The research and development communities are rapidly spinning up on exploiting DNB to help resolve difficulties in TC forecasting, and we anticipate that new/enhanced decision aids are close at hand.

The DNB is slated for four missions of the Joint Polar Satellite System (JPSS). JPSS-1 is slated to launch in fall 2017 and will be followed by three subsequent launches approximately every 5 years. DNB-like capabilities on GEO platforms have been formulated (Glumb et al. 2016) with excellent spatial resolution (~1 km), and this capability would aid the scientific community in closing the gap that currently exists between daytime and nighttime observations.

ACKNOWLEDGMENTS. Support of the NOAA JPSS Proving Ground and Risk Reduction Program (Grant NA14OAR4320125 Amd 7) and the Naval Research Laboratory (Grant N00173-14-G902) and the Oceanographer of the Navy through office at the PEO C4I and Space/PMW-120 under Program Element PE-0603207N is gratefully acknowledged. We thank Josh Cossuth for input to an early version of this manuscript and Derrick Herndon for his insightful reviews.

REFERENCES

Alexander, M. J., and Coauthors, 2010: Recent developments in gravity-wave effects in climate models and the global distribution of gravity wave momentum flux from observations and models. *Quart. J. Roy. Meteor. Soc.*, **136**, 1103–1124, doi:10.1002/qj.637.

Bankert, R. L., J. E. Solbrig, T. F. Lee, and S. D. Miller, 2011: Automated lightning flash detection in nighttime visible satellite data. *Wea. Forecasting*, **26**, 399–408, doi:10.1175/WAF-D-10-05002.1.

Cossuth, J., R. E. Hart, J. D. Hawkins, C. S. Velden, and A. Wimmers, 2014: Climatological analysis of tropical cyclone eye and inner-core structure from a global satellite-based passive microwave dataset. *31st Conf. on Hurricanes and Tropical Meteorology*, San Diego, CA, Amer. Meteor. Soc., 14. [Available online at https://ams.confex.com/ams/31Hurr/webprogram/Paper244730.html.]

Croft, T. A., 1978: Night-time images of the Earth from space. *Sci. Amer.*, **239**, 86–98, doi:10.1038/scientificamerican0778-86.

Dvorak, V. F., 1984: Tropical cyclone intensity analysis using satellite data. NOAA Tech. Rep. 11, 45 pp.

Eather, R. H., 1979: DMSP calibration. *J. Geophys. Res.*, **84**, 4134–4144, doi:10.1029/JA084iA08p04134.

Elvidge, C. D., K. E. Baugh, E. A. Kihn, H. W. Kroehl, and E. R. Davis, 1997: Mapping city lights using DMSP Operational Linescan System data. *Photogramm. Eng. Remote Sens.*, **63**, 727–734.

——, ——, J. B. Dietz, T. Bland, P. C. Sutton, and H. W. Kroehl, 1999: Radiance calibration of DMSP-OLS low-light imaging data of human settlements. *Remote Sens. Environ.*, **68**, 77–88.

Figa-Saldana, J., J. J. W. Wilson, E. Attema, R. Gelsthorpe, M. R. Drinkwater, and A. Stoffelen, 2002: The advanced scatterometer (ASCAT) on the meteorological operational (MetOp) platform: A follow on for European wind scatterometers. *Can. J. Remote Sens.*, **28**, 404–412, doi:10.5589/m02-035.

Gaiser, P. W., and Coauthors, 2004: The WindSat spaceborne polarimetric microwave radiometer: Sensor description and early orbit performance. *IEEE Trans.*

Geosci. Remote Sens., **42**, 2347–2361, doi:10.1109/TGRS.2004.836867.

Glumb, R. J., P. C. Griffith, P. Mantica, and D. Jordan, 2016: The ABI-based combined sounder/imager (CSI). *21st Conf. on Satellite Meteorology, Oceanography, and Climatology*, Madison, WI, Amer. Meteor. Soc., 9.1. [Available online at https://ams.confex.com/ams/21SATMET20ASI/webprogram/Paper297053.html.]

Hawkins, J. D., and C. Velden, 2011: Supporting meteorological field experiment missions and post-mission analysis with satellite digital data and products. *Bull. Amer. Meteor. Soc.*, **92**, 1009–1022, doi:10.1175/2011BAMS3138.1.

——, T. F. Lee, J. Turk, C. Sampson, J. Kent, and K. Richardson, 2001: Real-time Internet distribution of satellite products for tropical cyclone reconnaissance. *Bull. Amer. Meteor. Soc.*, **82**, 567–578, doi:10.1175/1520-0477(2001)082<0567:RIDOSP>2.3.CO;2.

——, F. J. Turk, T. F. Lee, and K. Richardson, 2008: Observations of tropical cyclones with the SSMIS. *IEEE Trans. Geosci. Remote Sens.*, **46**, 901–912, doi:10.1109/TGRS.2008.915753.

——, and Coauthors, 2014: Satellite-based tropical cyclone monitoring capabilities. *31st Conf. on Hurricanes and Tropical Meteorology*, San Diego, CA, Amer. Meteor. Soc., 10C.1. [Available online at https://ams.confex.com/ams/31Hurr/webprogram/Paper244006.html.]

Hendricks, E. A., M. T. Montgomery, and C. A. Davis, 2004: The role of "vertical" hot towers in the formation of tropical cyclone Diana (1984). *J. Atmos. Sci.*, **61**, 1209–1232, doi:10.1175/1520-0469(2004)061<1209:TROVHT>2.0.CO;2.

Hillger, D., and Coauthors, 2015: User validation of VIIRS satellite imagery. *Remote Sens.*, **2016**, 11, doi:10.3390/rs8010011.

Hollinger, J. P., 1989: DMSP Special Sensor Microwave/Imager calibration/validation. Naval Research Laboratory Space Sensing Branch Final Rep., Vol. I, 314 pp. [Available online at www.dtic.mil/dtic/tr/fulltext/u2/a274626.pdf.]

Kossin, J. P., B. D. McNoldy, and W. H. Schubert, 2002: Vortical swirls in hurricane eye clouds. *Mon. Wea. Rev.*, **130**, 3144–3149, doi:10.1175/1520-0493(2002)130<3144:VSIHEC>2.0.CO;2.

Kurihara, Y., M. A. Bender, and R. J. Ross, 1993: An initialization scheme of hurricane models by vortex specification. *Mon. Wea. Rev.*, **121**, 2030–2045, doi:10.1175/1520-0493(1993)121<2030:AISOHM>2.0.CO;2.

Lee, T. F., 2000: Nighttime observation of sheared tropical cyclones using GOES 3.9-μm data. *Wea. Forecasting*, **15**, 759–766, doi:10.1175/1520-0434(2000)015<0759:NOOSTC>2.0.CO;2.

——, F. J. Turk, J. D. Hawkins, and K. A. Richardson, 2002: Interpretation of TRMM TMI images of tropical cyclones. *Earth Interact.*, **6**, doi:10.1175/1087-3562(2002)006<0001:IOTTIO>2.0.CO;2.

——, S. D. Miller, F. J. Turk, C. Schueler, R. Julian, S. Deyo, P. Dills, and S. Wang, 2006: The NPOESS VIIRS day/night visible sensor. *Bull. Amer. Meteor. Soc.*, **87**, 191–199, doi:10.1175/BAMS-87-2-191.

Leslie, L. M., and G. Holland, 1995: On the bogussing of tropical cyclones in numerical models: A comparison of vortex profiles. *Meteor. Atmos. Phys.*, **56**, 101–110, doi:10.1007/BF01022523.

Liang, C. K., S. Mills, B. I. Hauss, and S. D. Miller, 2014: Improved VIIRS day/night band imagery with near-constant contrast. *IEEE Trans. Geosci. Remote Sens.*, **52**, 6964–6971, doi:10.1109/TGRS.2014.2306132.

Malkus, J. S., 1959: Recent development in studies of penetrative convection and an application to hurricane cumulonimbus towers. *Cumulus Dynamics*, C. Anderson, Ed., Pergamon Press, 65–84.

Miller, S. D., and R. E. Turner, 2009: A dynamic lunar spectral irradiance data set for NPOESS/VIIRS day/night band nighttime environmental applications. *IEEE Trans. Geosci. Remote Sens.*, **47**, 2316–2329, doi:10.1109/TGRS.2009.2012696.

——, C. L. Combs, S. Q. Kidder, and T. F. Lee, 2012a: Assessing moonlight availability for nighttime environmental applications by low-light visible polar-orbiting satellite sensors. *J. Atmos. Oceanic Technol.*, **29**, 538–557, doi:10.1175/JTECH-D-11-00192.1.

——, S. P. Mills, C. D. Elvidge, D. T. Lindsey, T. F. Lee, and J. D. Hawkins, 2012b: Suomi satellite brings to light a unique frontier of nighttime environmental sensing capabilities. *Proc. Natl. Acad. Sci. USA*, **109**, 15 706–15 711, doi:10.1073/pnas.1207034109.

——, and Coauthors, 2013: Illuminating the capabilities of the *Suomi National Polar-Orbiting Partnership* (NPP) Visible Infrared Imaging Radiometer Suite (VIIRS) day/night band. *Remote Sens.*, **5**, 6717–6766, doi:10.3390/rs5126717.

——, ——, J. Yue, S. M. Smith, M. J. Alexander, L. Hoffmann, M. Setvak, and P. T. Partain, 2015: Upper atmospheric gravity wave details revealed in nightglow satellite imagery. *Proc. Natl. Acad. Sci. USA*, **112**, 6728–6735, doi:10.1073/pnas.1508084112.

Mills, S., E. Jacobson, J. Jaron, J. McCarthy, T. Ohnuki, M. Plonski, D. Searcy, and S. Weiss, 2010: Calibration of the VIIRS day/night band (DNB). *Sixth Annual Symp. on Future National Operational Environmental Satellite Systems—NPOESS and GOES-R*, Atlanta, GA, Amer. Meteor. Soc., 9.4.

[Available online at https://ams.confex.com/ams/pdfpapers/163765.pdf.]

Olander, T., and C. Velden, 2007: The advanced Dvorak technique: Continued development of an objective scheme to estimate tropical cyclone intensity using geostationary infrared satellite imagery. *Wea. Forecasting*, **22**, 287–298, doi:10.1175/WAF975.1.

Orville, R. E., 1981: Global distribution of midnight lightning—September to November 1977. *Mon. Wea. Rev.*, **109**, 391–395, doi:10.1175/1520-0493(1981)109<0391:GDOMLT>2.0.CO;2.

Schueler, C., T. F. Lee, and S. D. Miller, 2013: VIIRS constant spatial-resolution advantages. *Int. J. Remote Sens.*, **34**, 5761–5777, doi:10.1080/01431161.2013.796102.

Simpson, J., J. B. Halverson, B. S. Ferrier, W. A. Peterson, R. H. Simpson, R. Blakeslee, and S. L. Durden, 1998: On the role of "hot towers" in tropical cyclone formation. *Meteor. Atmos. Phys.*, **67**, 15–35, doi:10.1007/BF01277500.

Turk, F. J., S. DiMichele, and J. D. Hawkins, 2006: Observations of tropical cyclone structure from WindSat. *IEEE Trans. Geosci. Remote Sens.*, **44**, 645–655, doi:10.1109/TGRS.2006.869926.

Velden, C. S., and J. Sears, 2014: Computing deep-tropospheric vertical wind shear analyses for tropical cyclone applications: Does the methodology matter? *Wea. Forecasting*, **29**, 1169–1180, doi:10.1175/WAF-D-13-00147.1.

——, T. Olander, and R. M. Zehr, 1998: Development of an objective scheme to estimate tropical cyclone intensity from digital geostationary satellite imagery. *Wea. Forecasting*, **13**, 172–186, doi:10.1175/1520-0434(1998)013<0172:DOAOST>2.0.CO;2.

——, and Coauthors, 2006: The Dvorak tropical cyclone intensity estimation technique: A satellite-based method that has endured for over 30 years. *Bull. Amer. Meteor. Soc.*, **87**, 1195–1210, doi:10.1175/BAMS-87-9-1195.

Welch, R., 1980: Monitoring urban population and energy utilization patterns from satellite data. *Remote Sens. Environ.*, **9**, 1–9, doi:10.1016/0034-4257(80)90043-7.

Wimmers, A. J., and C. S. Velden, 2010: Objectively determining the rotational center of tropical cyclones in passive microwave satellite imagery. *J. Appl. Meteor. Climatol.*, **49**, 2013–2034, doi:10.1175/2010JAMC2490.1.

——, and ——, 2016: Advancements in objective multisatellite tropical cyclone center fixing. *J. Appl. Meteor. Climatol.*, **55**, 197–212, doi:10.1175/JAMC-D-15-0098.1.

Yue, J., S. D. Miller, L. Hoffmann, and W. C. Straka III, 2014: Stratospheric and mesospheric concentric gravity waves over tropical cyclone Mahasen: Joint AIRS and VIIRS satellite observations. *J. Atmos. Sol.-Terr. Phys.*, **119**, 83–90, doi:10.1016/j.jastp.2014.07.003.

Zipser, E. J., 2003: Some views on "hot towers" after 50 years of tropical field programs and two years of TRMM data. *Cloud Systems, Hurricanes, and the Tropical Rainfall Measuring Mission (TRMM)—A Tribute to Dr. Joanne Simpson*, *Meteor. Monogr.*, No. 40, Amer. Meteor. Soc., 49–58, doi:10.1175/0065-9401(2003)029<0049:CSVOHT>2.0.CO;2.

Attend the AMS 98th Annual Meeting in Austin, TX from 7–11 January, 2018

This year's theme is

Transforming Communication in the Weather, Water, and Climate Enterprise

Don't miss 30+ conferences and symposia, networking opportunities, short courses, and hundreds of exhibitors. Early registration deadline is 1 December.

AMS
American Meteorological Society
98th Annual Meeting | AUSTIN | 2018
www.annual.ametsoc.org/2018